Materials Chemistry Frontiers

ROYAL SOCIETY OF CHEMISTRY

COMMUNICATION

FRET-mediated near infrared whispering gallery modes: Studies on the relevance of intracavity energy transfer with Q-factor

Osamu Oki,[a] Soh Kushida,[a] Annabel Mikosch,[b] Kota Hatanaka,[c] Youhei Takeda,[c] Satoshi Minakata,[c] Junpei Kuwabara,[a,d] Takaki Kanbara,[a,d] Thang D. Dao,[e] Satoshi Ishii,[e] Tadaaki Nagao,[e] Alexander J. C. Kuehne,[b] Felix Deschler,[f] Richard Friend,[f] and Yohei Yamamoto*[a,d]

Near infrared (NIR) optical microsphere resonators are prepared by coassembly of energy-donating and accepting conjugated polymers. In the microspheres, fluorescence resonance energy transfer occurs, leading to sharp and periodic photoluminescence from whispering gallery modes in the NIR region with Q-factors as high as 600.

Near infrared (NIR) emitting materials represent powerful tools for biosensing and light source for bioimaging due to the high transparency of biological organisms in this spectral window.[1] Therein, NIR luminescent colloidal probes with sharp emission lines are often utilized. Recently, polymer whispering gallery mode (WGM) microresonators with narrow luminescence and laser emission have been reported.[2] Furthermore, π-conjugated organic and polymer microparticles, in some cases doped with rare-earth metals, were shown to exhibit resonant emission and lasing in the visible and NIR region.[2,3] Such organic microresonators find applications for barcoding in live cells, where lasing with a unique spectral profile makes it possible to distinguish each cell.[4] However, NIR emitters often suffer from low luminescence efficiency because of the small energy gap between highest-occupied and lowest-unoccupied molecular orbitals (HOMO and LUMO, respectively) that causes non-radiative thermal deactivation.[5] Furthermore, aggregation of molecules often causes serious quenching of the NIR emission.

The absence of high-performance organic and polymeric lasers in the NIR spectral regime hinders the development of new biomedical imaging probes as well as NIR communication sources. Advancing polymeric microsphere lasers into the NIR spectral region would open up numerous applications in biological systems.

Fluorescence resonance energy transfer (FRET) is an energy transfer mechanism that yields down-converted photoluminescence (PL) with high efficiency.[6] Because the effective distance of FRET is typically within 10 nm,[6] molecules that interchange energy have to be blended homogeneously without macroscopic phase separation.[7] Recently, we reported color conversion of WGM PL in microsphere resonators consisting of two blended π-conjugated polymers. By utilizing FRET, effective red-shifted WGM PL was achieved in the microsphere resonators.[8]

In this communication, we realize FRET in blended conjugated polymer microspheres that leads to NIR emission

a. Division of Materials Science, Faculty of Pure and Applied Sciences, University of Tsukuba, 1-1-1 Tennodai, Tsukuba, Ibaraki 305-8573, Japan.
b. DWI–Leibniz Institute for Interactive Materials, RWTH Aachen University, Forckenbeckstraße 50, 52076 Aachen, Germany.
c. Department of Applied Chemistry, Graduate School of Engineering, Osaka University, 2-1 Yamadaoka, Suita, Osaka 565-0871, Japan.
d. Tsukuba Research Center for Energy Materials Science (TREMS), University of Tsukuba, 1-1-1 Tennodai, Tsukuba, Ibaraki 305-8573, Japan.
e. Nano-System Photonics Group, Nano-System Organization Unit, National Institute for Materials Science (NIMS), 1-1 Namiki, Tsukuba, Ibaraki, 305-0044 Japan.
f. Cavendish Laboratory, University of Cambridge, JJ Thomson Avenue, CB3 0HE Cambridge, UK.
† Footnotes relating to the title and/or authors should appear here.
Electronic Supplementary Information (ESI) available: [details of any supplementary information available should be included here]. See DOI: 10.1039/x0xx00000x
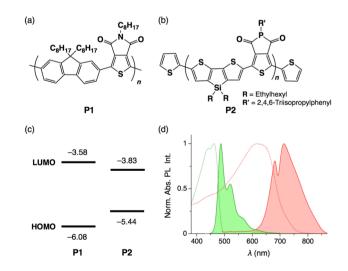
Fig. 1. Chemical structures of **P1** (a) and **P2** (b). (c) HOMO and LUMO energy levels of **P1** and **P2** with respect to the vacuum level. (d) Photoabsorption (broken lines) and PL (solid lines) spectra of **P1** (green) and **P2** (red) in CHCl$_3$.
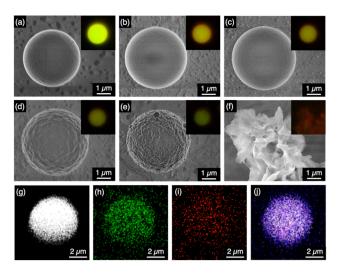
Fig. 2. (a–f) SEM micrographs of the self-assembled precipitates of **P1** and **P2** with f_{P2} = 0 (a), 0.03 (b), 0.04 (c), 0.07 (d), 0.1 (e), and 1 (f). Insets show fluorescent micrographs of the precipitates. Image size: 10 x 10 μm. λ_{ex} = 400–440 nm. (g–j) EDS mapping images of the self-assembled microsphere with f_{P2} = 0.04 on an aluminum stage. (g) C $K\alpha_1$ and $K\alpha_2$, (h) Si $K\alpha_1$, (i) P $K\alpha_1$, (j) S $K\alpha_1$.

Fig. 3. (a) Bar graph of ϕ_{PL} (λ_{PL} = 500–900 nm) and its red-to-NIR fraction (λ_{PL} = 650–900 nm, red) versus f_{P2} of cast films of the self-assembled precipitates (microspheres for f_{P2} = 0–0.1 and irregular aggregates for f_{P2} = 1). λ_{ex} = 470 nm. (b) Plots of the fraction of NIR PL to PL at all the wavelength region versus f_{P2} for cast films of the microspheres (closed squares) and a single microsphere (open squares). (c) PL spectra of a single microsphere of **P1** and **P1/P2** blends with f_{P2} = 0–0.2 upon focused laser irradiation at 470 nm. (d) PL decay profiles at λ_{PL} = 540 nm (±2.5 nm range) of a single microsphere with f_{P2} = 0 (black), 0.01 (red), 0.02 (orange), 0.04 (green), and 0.07 (blue). λ_{ex} = 470 nm. Insets show plots of $\tau_{1/2}$ versus f_{P2} at λ_{PL} = 540 nm (±2.5 nm range). The plots are the average value with the measurements of 5–7 isolated microspheres. (e) Plot of γ versus f_{P2}.

from a WGM cavity. The polymers we used in this study, named **P1** and **P2**, act as an energy donor and acceptor, respectively. **P2** displays PL at red-to-NIR region in solution but hardly fluoresces in the solid state because of the aggregation quenching. By contrast, microspheres formed by coassembly of **P1** and small fraction of **P2** exhibit clear WGM PL in the NIR spectral region, resulting from efficient intrasphere FRET from **P1** to **P2**. The utilization of FRET inside a microresonator is useful to efficiently extract NIR light with narrow line width.

The π-conjugated polymers, **P1** (poly[(9,9-dioctylfluorene-2,7-diyl)-*alt*-(5-octylthieno[3,4-*c*]pyrrole-4,6-dione-1,3-diyl)] with number-average molecular weight (M_n) of 24 kg mol^{-1}, Fig. 1a) and **P2** (poly[(5-(2,4,6-triisopropylphenyl)thieno[3,4-*c*]phosphole-4,6-dione)-*alt*-(4,4-bis(2-ethylhexyl)-silolo-[3,2-*b*:4,5-*b*']dithiophene)] , M_n = 6.5 kg mol^{-1}, Fig. 1b) were synthesized according to reported procedures.[9] The HOMO and LUMO energy levels are −6.08 and −3.58 eV for **P1** and −5.44 and −3.83 eV for **P2**, respectively, with respect to the vacuum level (Fig. 1c). As shown in the photoabsorption and PL spectra of **P1** and **P2** in CHCl$_3$, the PL band of **P1** largely overlaps with the absorption band of **P2**, indicating that efficient FRET from **P1** to **P2** is possible (Fig. 1d). Indeed, in cast films prepared by spin coating of **P1** and **P2** in CHCl$_3$ solution, PL from **P1** is mostly quenched even when the weight fraction of **P2** (f_{P2}) is only 0.02 (Fig. S1).

Self-assembly of **P1** and **P2** and coassembly of their blends into WGM microsphere resonators were carried out by slow diffusion of MeOH vapour into their CHCl$_3$ solutions (see the experimental section).[2,10] The total initial concentration of polymers **P1** and/or **P2** was set at 0.5 mg mL^{-1}. After three days of vapour diffusion at 25 °C, the solution changed to a suspension, and the polymers were precipitated. Scanning
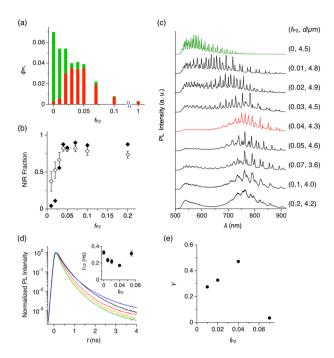
electron microscopy (SEM) shows that **P1** (f_{P2} = 0) forms well-defined microspheres with a typical diameter of 5 μm (Fig. 2a),[2a,8,11] while **P2** (f_{P2} = 1) gave irregular aggregates (Fig. 2f). For **P1/P2** blend, well-defined microspheres with smooth surface morphology could be obtained within a f_{P2} range of 0.01–0.05 (Fig. 2b, c). However, in case of the coassembly with f_{P2} greater than 0.06, the surface morphology of the resulting spheres deteriorated (Fig. 2d, e). Polymer blends tend to phase separate due to their small mixing entropy.[7] In case of f_{P2} ≥ 0.06, microspheres with rough surfaces are obtained with characteristic features inherent to phase segregation. On the other hand, in case of f_{P2} ≤ 0.05, **P1** and **P2** are well mixed, and segregation of **P2** is suppressed due to its small fraction. In fact, energy dispersive X-ray spectrometry (EDS) mapping of the microsphere with f_{P2} = 0.04 shows that signals of Si and P from **P2** are homogeneously distributed throughout the entire microsphere. This result indicates that **P2** is well dispersed in a single microsphere (Figure 2g–j). The signals of each element

COMMUNICATION

are much clearer for microspheres with f_{P2} = 0.07, yet it is hard to recognize the phase separation of **P1** and **P2**, because the resolution of the apparatus is not sufficient (Fig. S3).

The change of PL quantum yield (ϕ_{PL}) with f_{P2} further indicates that **P2** is well dispersed in the **P1** matrix. Upon excitation at 470 nm, ϕ_{PL} of the microspheres decreases monotonically with increasing f_{P2} (Fig. 3a). However, the fraction of the PL in the red and NIR region (λ = 650–950 nm) increases with increasing f_{P2}, and at $f_{P2} \geq 0.03$, the PL spectrum is same as for pure **P2** (Fig. 3b, closed squares). These results show that efficient energy transfer takes place from **P1** to **P2**. When f_{P2} is greater than 0.07, ϕ_{PL} decreases largely, indicating that the aggregation of **P2** causes concentration quenching of the NIR PL from **P2**. Excitation specturum of a cast film of microspheres (f_{P2} = 0.05) shows that PL at 650 nm is mostly generated by photoabsorption of **P1**, further supporting that efficient energy transfer from **P1** to **P2** occurs inside the microsphere (Fig. S2).

To quantify the energy transfer, we measure PL spectra of individual microspheres (λ_{ex} = 470 nm, see the experimental section and Fig. S4). For microspheres with f_{P2} = 0–0.2, characteristic spectral modulation from the WGM cavity can be observed, indicating that the generated PL is confined inside of the microspheres and self-interferes (Fig. 3c).[2,8,12] As f_{P2} increases, the spectral series of WGM modes shift from the visible to the NIR region, and at f_{P2} = 0.04, WGM PL is observed mostly in the NIR region at 700–900 nm (Fig. 3c, red). According to the area intensity, more than 80% of the PL originates from **P2** in the microsphere with f_{P2} of 0.04 (Fig. 3b, open circles). At f_{P2} greater than 0.07, the NIR PL slightly decreases and the PL in the visible region reappears (Fig. 3c), possibly caused by the meso- and macroscopic phase segregation of **P1** and **P2** in the microsphere (Fig. 2d and e).

We performed time-resolved PL spectroscopy, which further supports the intrasphere energy transfer. As f_{P2} increases from 0 to 0.04, the PL half lifetime ($\tau_{1/2}$) at 540 nm (PL from **P1**) monotonically decreases from 0.327 to 0.172 ns (Fig. 3d), while $\tau_{1/2}$ at 675–730 nm (PL from **P2**) is almost constant at around 0.6 ns (Fig. S5). Further increase of f_{P2} to 0.07 results in an increase of $\tau_{1/2}$ at 540 nm to 0.315 ns.

The energy transfer efficiency (γ) in the single microsphere is evaluated with equation (1),

$$\gamma = 1 - \tau_B/\tau_D \qquad (1)$$

where τ_D and τ_B represent the PL half lifetime of the energy donating polymer (λ_{PL} = 540 nm) in the microspheres of **P1** and **P1/P2** blend, respectively.[6b] We find that γ increases from 0.276 to 0.473 with increasing f_{P2} from 0.01 to 0.04 (Fig. 3e). However, further increase of f_{P2} to 0.07 greatly suppresses γ. The phase separation of **P1** and **P2** in the microsphere starts to occur at this blending fraction, which also reduces the donor-acceptor interface area in the microsphere.

We further carry on to determine the performance of the WGM resonator by evaluating the Q-factor. The average Q-factor is defined as the peak wavelength divided by the full-width at the half maximum of the observed WGM PL peaks (Q_{av}). For the microspheres with $f_{P2} \leq 0.07$ and d ~ 5 μm, Q_{av} is around 400 (Fig. 4a). With increasing $f_{P2} \geq 0.1$, Q_{av} decreases

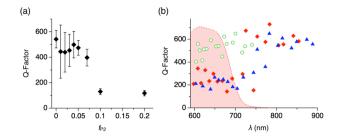**Fig. 4.** (a) Plot of the average Q-factor versus f_{P2}. (b) Plots of Q-factors of each WGM PL line for microspheres with f_{P2} = 0 (circle), 0.01 (square), and 0.02 (triangle). The red-colored area indicates photoabsorption spectrum of a CHCl$_3$ solution of **P2**.

greatly to ~100, which results from the increased surface roughness that causes scattering losses of the confined PL. It is noteworthy that the Q-factor shows wavelength dependency. The WGM PL lines of the microspheres with f_{P2} = 0 display Q-factors around 500 (Figs. 4b and S6, green).[13] By contrast, WGMs of the microspheres with f_{P2} = 0.01 and 0.02 exhibit Q-factors around 200 in the visible range (600–750 nm) and as large as 600 in the NIR region (> 800 nm, Figs. 4b and S6, red and blue). Q-factor is described as follows:

$$Q^{-1} = Q_{rad}^{-1} + Q_{scat}^{-1} + Q_{abs}^{-1} \qquad (2)$$

where Q_{rad}^{-1} is leakage loss for the internal reflection, Q_{scat}^{-1} is scattering loss by the surface roughness, and Q_{abs}^{-1} is absorption loss by the resonator medium.[13] Q_{abs}^{-1} is shown as

$$Q_{abs}^{-1} = \alpha\lambda/2n\pi \qquad (3)$$

where α is absorption coefficient and n is refractive index of the medium.[14] Q_{abs}^{-1} increases when λ overlaps with the absorption wavelength, thereby resulting in the decrease of Q. As shown in Figure 4b, the increase of the Q-factor is observed at wavelengths higher than 750 nm. This wavelength coincides with the absorption edge of the doped **P2** (Fig. 4b, blue and red). Using equation (3), we simulate the wavelength dependency of Q_{abs}, and the tendency of the experimental plot in Figure 4b matches well with the simulated plots (Fig. S7).

On the other hand, Q_{rad}^{-1} and Q_{scat}^{-1} of the compared microspheres are assumed not differ greatly, because microspheres with identical diameters (~ 5 μm) and similar degree of surface roughness are applied here. Q_{rad} is indeed size dependent,[14b] which is clearly visible when plotting Q versus the particle diameter (Fig. S8). As a result of the reabsorption loss, WGM lines in the visible range display smaller Q values (~200) than those in the NIR range, where they reach as high as 600. This value is of similar level as previously reported NIR WGMs of self-assembled organic resonators.[3]

Conclusions

We fabricate whispering gallery mode (WGM) microresonators by self-assembly of energy donating conjugated polymer doped with a small portion of energy accepting, NIR-emitting polymer. Due to efficient energy transfer (FRET) from donor to

acceptor polymers inside the microspheres, WGM in the NIR region appears upon photoexcitation at the perimeter of the microsphere. The observed Q-factor is as high as 600 in the NIR region, at which the absorption loss by the energy-accepting polymer is almost dismissed. The NIR WGM resonators will be valuable for applications as sensing and imaging in the biological system.[15]

Experimental section

Self-assembly of P1, P2 and coassembly of their blends. Typically, a 5 mL vial containing a CHCl$_3$ solution of **P1**, **P2** or their blends with a total concentration and amount of 0.5 mg mL^{-1} and 2 mL, respectively, was placed in a 50 mL vial containing 5 mL of MeOH. The outside vial was capped and then allowed to stand for 3 days at 25 °C. The vapour of the nonsolvent was slowly diffused into the solution, resulting in a precipitation of the polymers through the supersaturated state.

μ-PL Measurements. μ-PL measurements were carried out using a μ-PL measurement system (Fig. S4).[8] An optical microscope was used with a long-distance 100x objective (NA = 0.8) to identify suitable particles and determine their diameters. For measurements, a WITec μ-PL system was used with a model Alpha 300S microscope combined with a Princeton Instruments model Action SP2300 monochromator (grating: 300 grooves mm^{-1}) and an Andor iDus model DU-401A BR-DD-352 CCD camera cooled to –60 °C. The PL spectrum was measured at a resolution of 0.27 nm. The edge of a single sphere was photoexcited at 25 °C under ambient conditions by a diode pulsed laser (a PicoQuant model LDH-D-C-470B with a PDL 828 'Sepia II' driver) with the wavelength, power, integration time, frequency, pulse duration and spot size of 470 nm, 1.5 μW, 1 s, 2.5 MHz, 70 ps, and ~1 μm, respectively. Time-resolved PL decay experiments on individual isolated microspheres were carried out on the samples sealed under nitrogen in a glove box using a PicoHarp 300 TCSPC module from PicoQuant hooked to a Leica TCS SP8 microscope equipped with a pulsed White Light Laser.

Acknowledgements

Conflicts of interest

There are no conflicts to declare.

Author Contribution

YY and YT designed experiment, KH, YT, SM, JK, TK synthesized polymers, OO and SK conducted self-assembly, OO, AM, TD, SI, TN, AK, FD, RF conducted μ-PL and time-resolved PL measurements, YY and OO prepared manuscript.

Notes and references

1 (*a*) E. A. Owens, M. Henary, G. E. Fakhri, H. S. Choi, *Acc. Chem. Res*. 2016, **49**, 1731; (*b*) V. Pansare, S. Hejazi, W. Faenza, R. K. Prud'homme, *Chem. Mater*. 2012, **24**, 812; (*c*) Y. Koide, Y. Urano, K. Hanaoka, W. Piao, M. Kusakabe, N. Saito, T. Terai, T. Okabe, T. Nagano, *J. Am. Chem. Soc*. 2012, **134**, 5029.
2 (*a*) K. Tabata, D. Braam, S. Kushida, L. Tong, J. Kuwabara, T. Kanbara, A. Beckel, A. Lorke, Y. Yamamoto, *Sci. Rep*. 2014, **10**, 5902; (*b*) S. Ciftci, A. Mikosch, B. Haehnle, L. Witczak, A. J. C. Kuehne, *ChemComm* 2016, **52**, 14222; (*c*) S. Kushida, D. Okada, F. Sasaki, Z.-H. Lin, J.-S. Huang, Y. Yamamoto, *Adv. Opt. Mater*. 2017, **5**, 1700123.
3 (*a*) X. Wang, Q. Liao, H. Li, S. Bai, Y. Wu, X. Lu, H. Hu, Q. Shi, H. Fu, *J. Am. Chem. Soc*. 2015, **137**, 9289; (*b*) D. Venkatakrishnarao, R. Chandrasekar, *Adv. Opt. Mater.* 2016, **4**, 112; (*c*) D. Venkatakrishnarao, M. A. Mohiddon, R. Chandrasekar, *Adv. Opt. Mater.* 2017, **5**, 1600613, (d) Yemineni S. L. Narayana, D. Venkatakrishnarao, A. Biswas, M. A. Mohiddon, N. Viswanathan, R. Chandrasekar, *ACS Appl. Mater. Interfaces* 2016, **8**, 952-958.
4 M. Schubert, A. Steude, P. Liehm, N. M. Kronenberg, M. Karl, E. C. Campbell, S. J. Powis, M. C. Gather, *Nano Lett*. 2015, **15**, 5647.
5 (*a*) M. Shimizu, R. Kaki, Y. Takeda, T. Hiyama, N. Nagai, H. Yamagishi, H. Furutani, *Angew. Chem. Int. Ed*. 2012, **51**, 4095; (*b*) J. Massin, W. Dayoub, J.-C. Mulatier, C. Aronica, Y. Bretonniere, C. Andraud, *Chem. Mater.* 2011, **23**, 862; (*c*) O. Fenwick, J. Sprafke, J. Binas, D. Kondratuk, F. D. Stasio, H. L. Anderson, F. Cacialli, *Nano Lett*. 2011, **11**, 2451.
6 (*a*) V. T. Förster, *Annal. Phys*. 1948, **6**, 55; (*b*) J. P. S. Farinha, J. M. Martinho, *J. Phys. Chem. C* 2008, **112**, 10591.
7 C. Pan, K. Sugiyasu, M. Takeuchi, *Chem. Commun*. 2014, **50**, 11814.
8 S. Kushida, D. Braam, T. D. Dao, H. Saito, K. Shibasaki, S. Ishii, T. Nagao, A. Saeki, J. Kuwabara, T. Kanbara, M. Kijima, A. Lorke, Y. Yamamoto, *ACS Nano* 2016, **10**, 5543.
9 (*a*) H. Saito, J. Kuwabara, T. Kanbara, *J. Polym. Sci., Part A: Polym. Chem*. 2015, **53**, 2198; (*b*) Y. Takeda, K. Hatanaka, T. Nishida, S. Minakata, *Chem. Eur. J*. 2016, **22**, 10360.
10 T. Adachi, L. Tong, J. Kuwabara, T. Kanbara, A. Saeki, S. Seki, Y. Yamamoto, *J. Am. Chem. Soc*. 2013, **135**, 870.
11 S. Kushida, O. Oki, H. Saito, J. Kuwabara, T. Kanbara, M. Tashiro, M. Katouda, Y. Imamura, Y. Yamamoto, *J. Phys. Chem. Lett*. 2017, **10**, 4580.
12 S. Kushida, D. Braam, C. Pan, T. Dao, K. Tabata, K. Sugiyasu, M. Takeuchi, S. Ishii, T. Nagao, A. Lorke, Y. Yamamoto, *Macromolecules* 2015, **48**, 3928.
13 a) S. Schiller, *Appl. Opt*. 1993, **32**, 2181. b) L. L. Martín, P. Haro-González, I. R. Martín, D. Navarro-Urrios, D. Alonso, C. Pérez-Rodríguez, D. Jaque, N. E. Capuj, *Opt. Lett*. 2011, **36**, 615.
14 (*a*) I. Alvarado-Rodrigues, E. Yablonovitch, *J. Appl. Phys.* 2002, **92**, 6399; (*b*) M. L. Gorodetsky, A. A. Savchenkov, V. S. Ilchenko, *Opt. Lett*. 1996, **21**, 453.
15 M. R. Foreman, J. D. Swaim, F. Vollmer, *Adv. Opt. Photon*. 2015, **7**, 168.